Landslides (2018) 15:2061–2073
DOI 10.1007/s10346-018-1041-x
Received: 19 May 2018
Accepted: 13 July 2018
Published online: 20 July 2018

Shi-lin Zhang · Zhao-hui Zhu · Shun-chao Qi · Yu-xiang Hu · Qing Du · Jia-wen Zhou

Deformation process and mechanism analyses for a planar sliding in the Mayanpo massive bedding rock slope at the Xiangjiaba Hydropower Station

Abstract Planar sliding, which has a universal characteristic of existing planar discontinuities, is very common in nature. The Mayanpo slope, a massive bedding rockslide, typical planar sliding, exploiting a sedimentary formation of interbedded sandstone and argillaceous stratums mixed with four strongly weathered weak interlayers, presents creep deformation that has interrupted the construction of the Xiangjiaba Hydropower Station. Field investigations indicate that the deformation behavior of Mayanpo slope should be analyzed within two different zones, namely zone I (east side) and zone II (west side). Although both zones are primarily controlled by the bottom weak interlayer (JC-1), the deformation magnitudes and potential failure modes are different: (a) Zone I exhibits a deformation that is significantly larger in magnitude than zone II, and (b) zone I and zone II present multistage and integral creep-fracturing progressive deformation-failure mode, respectively. The mechanism of this creep deformation can be considered to be the endogenic and exogenic integration. The progressive degradation of predominant discontinuity from primary soft rock stratum to weak interlayer is the fundamental which provides the possibility of kinematic release. The numerical analysis conducted with hydromechanical finite difference method (FDM) shows that excavation without reinforcement and rainfall can (i) enable kinematic feasibility and creep deformation, (ii) trigger the ceaseless propagation of sliding zone along JC-1, and (iii) promote the formation of a tensile strain concentration zone in the trailing under tension-shear effect. Furthermore, discussions on the engineering core measures for prevention and control are presented, which have important implications for similar engineering projects.

Keywords Planar sliding · Massive bedding rock slope · Weak interlayer · Deformation characteristics · Deformation mechanism

Introduction

Long-term geological effects and short-term environmental conditions can cause the down-slope transport of soil and rock, i.e., landslides, including deep-seated sliding/failure, shallow sliding/failure and rockfall, which can lead to great economic losses and causalities (Leshchinsky et al. 2015; Zhou et al. 2016). Among the different types of slope failure, planar sliding is a common type with a universal characteristic of existing planar discontinuities (e.g., faults, joints, bedding surfaces, and weak intercalated layers) (Hungr et al. 2014). The behavior of slope deformation is controlled by the predominant discontinuities, over which the sliding mass moves downwards and outwards if catastrophe failure occurred eventually (Lynn and Peter 2008; Ghazvinian et al. 2010; Hungr et al. 2014). Summarizing the generalities from previous researches on this kind of sliding, the evolution of predominant discontinuities is associated with planar sliding under external and internal disturbances (such as rainfall, undercutting by excavation and tectonic movement), which can be summarized as the progressive degradation of mechanical properties of predominant discontinuities and the propagation of sliding zone (Hatzor and Levin 1997; Haruo 2001; Wen and Aydin 2005; Xu et al. 2015; Havaej and Stead 2016; Tannant et al. 2017). Once failed, this kind of sliding has great damage capability, because of the possibility of high-speed remote motion as reported in the spectacular case study on the Seymareh rock avalanche by Roberts and Evans (2013).

The study on the characteristics and formations of planar sliding is a prerequisite to the appropriate identification and cognition of deformation-failure geomechanics model. The planar sliding is a time-dependent process usually presenting creep characteristics under gravity (Hart 2000). This kind of planar sliding can occur at various scales on strata along discontinuous surfaces, even when the slope gradients are quite gentle (Cruden and Antoine 1984). From a large number of cases, Hart (2000) suggested that the main preparatory factor leading to planar sliding is the presence of a pre-existing bedding-parallel shear zone, which forms the basic rupture surface for the potential sliding masses. The triggering factors for coalescence of dominant discontinuities vary, e.g., undercut by either erosion or excavation, and degradation of mechanical properties (Yue and Lee 2002; Eberhardt et al. 2004; Eberhardt et al. 2005; Roberts and Evans 2013; Xu et al. 2015).

China is one of the most landslide-prone countries in the world, especially in the southwestern region. This is not only due to the fragile geological environment, heavy rainfall, and strong earthquake, but also frequent artificial disturbances of numerous engineering activities during the Great Western Development Strategy. As a consequence, landslides occur in an endless stream (Huang 2007; Zhou et al. 2016). Previous works suggested that planar sliding is one of the most common types. Yin et al. (2016a) found that planar slides account for more than half of the large-scale slides in the Three Gorges Reservoir area. Many landslides triggered by the Wenchuan earthquake were also of this type (Xu et al. 2014), such as the Tangjiashan bedding rock landslide. In these planar slides, the massive bedding rock slopes, consisting of a sedimentary formation of interbedded weathered rock stratum (e.g., sandstone, mudstone, shale, marl, and limestone) mixed with predominant discontinuities (e.g., muddy intercalation, carbonaceous shale intercalation and carbonatite intercalation) are very common. Influenced by these predominant discontinuities, this kind of slope behaves anisotropically and acts as weak planes (Stead and Wolter 2015), and because of unfavorable physical and mechanical properties, these discontinuities have an obvious evolutionary process (Yin et al. 2011; Tang et al. 2015; Zhou et al. 2017), during which the continuous weakening of predominant discontinuities makes lots of contribution to the kinematical

release. In this study, the Mayanpo massive bedding rock slope, which presented creep deformation and posed a great threat to the construction of the Xiangjiaba Hydropower Station, is taken as an example to systematically study the deformation behavior, triggering mechanism, and prevention measures.

Background

The Xiangjiaba Hydropower Station is located on the lower reaches of the Jinsha River, which is close to the Shuifu County, Yunnan Province, China. The constriction commenced in 2006 and was completed in 2014. As one of the core parts of the temporary construction site, the Mayanpo slope is located on the right bank of the dam, as shown in Fig. 1(a). In the early stage of the construction of the Xiangjiaba Hydropower Station, many temporary facilities and buildings were placed on the Mayanpo slope, as shown in Fig. 1(b). The deformation of the Mayanpo slope has significantly affected and interrupted the engineering construction activities and caused great economic losses. Combining with field geological investigation, the settings will be introduced in this section firstly.

Geomorphological characteristics

As shown in Fig. 1(b, c), the fluctuation of elevation of the Mayanpo slope in the range from elevation (EL) 300.0 m to EL. 624.0 m is not apparent in the south-north region. In the east-west region, a gully (named the Mayan gully in Fig. 1(a)), at the elevation of 350.0–500.0 m, cuts through the slope. In the western part of the slope, the strike is approximately parallel to the Mayan gully with around 70°–80°. However, influenced by the incised action of an ancient riverbed, the strike in the eastern is approximately 60°–70°. The Mayanpo slope has an average slope gradient of 12°–20°. The slopes in this area differ spatially due to the effect of deep erosion from both the Mayan gully and the Jinsha River. The slope gradient is relatively steeper both near the Mayan gully and in the west, while the slope gradient gradually becomes gentler with increase in the elevation. Due to the excavation for foundations and roads, several multistep steps with the slope gradients from 1:0.75 to 1:0.5 and the heights from a few to several dozens of meters were formed, as shown in Fig. 1(d).

Geological characteristics and partition

The Mayanpo slope is a typical monoclinic stratum; the attitude of the rock stratum reveals a N60°-80°E strike, SE dip direction, and dip angle of 12°–25°. According to the field investigation (geotechnical mapping and drilling exploration (Fig. 2(a))), the rock units explored in the Mayanpo slope primarily consist of Jurassic sediments belonging to middle-lower Ziliujing group exploiting a formation of interbedded argillaceous rock and sandstone, and the bedding planes are approximately parallel to the surface. The area at a depth from 0 to 6.4 m is composed of Quaternary qesl and deluvium, mainly including sandy soil and fragment stone,

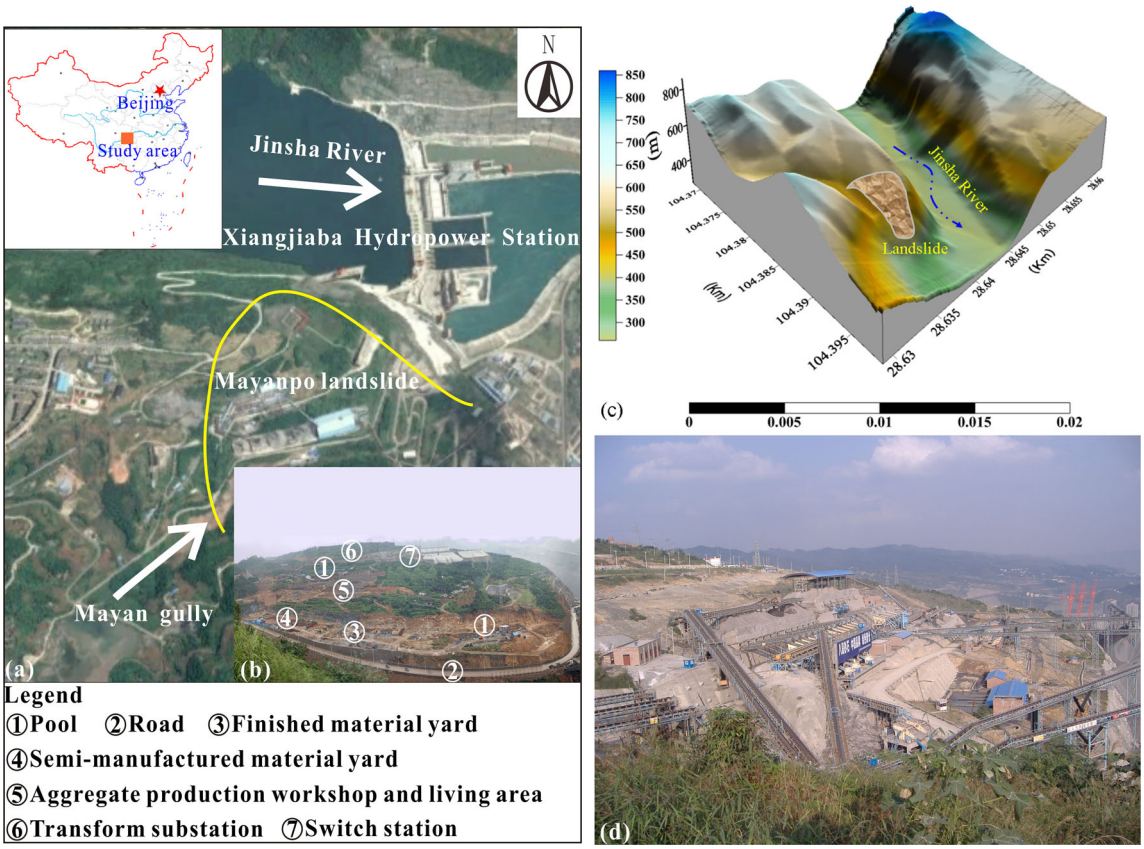

Fig. 1 Locations, terrain characteristics and distribution of temporary facilities and buildings on the Mayanpo slope: (a) location and regional terrain features, (b) distribution of temporary facilities and buildings on the Mayanpo slope during construction of the Xiangjiaba Hydropower Station, (c) a three-dimensional visualization of the study area and (d) multistep steps formed by excavation

below which respectively are gray and light yellow medium thick-layered medium fine-grained sandstone mixed with tan and brick red thin-layered fine-grained sandstone and argillaceous rock with the thickness of 10 to 28 m, and gray argillaceous rock comprised of argillaceous siltstone, silty mudstone, and mudstone intercalated siltstone. These characteristics of bedding plane are mapped in Fig. 2(b) (section I) and (c) (section II).

Weathering and stress release play vital roles in the development of rock stratum. The thick layer of sandstone in the upper part with persistence resisting weathering has led to the weathering layer within a relatively shallow depth (i.e., strong and/or medium weathered layers with the thicknesses of 4–10 m and 15–20 m, respectively). There are lots of thin-layered rock strata in the upper part that can easily evolve into strongly weathered interlayers, some of which have been slimed into weak interlayered layers due to low resistance to weathering. With the increase of depth, the bottom argillaceous rocks are insignificantly affected by weathering and remain basically as fresh rock mass.

According to geomorphological, geological, and deformation characteristics, the Mayanpo slope can be best analyzed in two zones, i.e., zone I and II at east and west sides, respectively, as labeled in Fig. 2(a). The diversities of geomorphology mainly refer to the differences in the east-west region as introduced in previous section. The differences in terms of geology are primarily illustrated by the rock quality according to field investigation. According to the drilling exploration, the recorded rock quality designation (RQD) which can be used as designation in classification of rock integrity and the development of fissure indicates that the argillaceous rock strata for zone I and zone II are similar, while the values of RQD of sandstone stratum in zone I (with an average value of 29.7%) are much higher than that in zone II (average value of 13%) (Fig. 3), which indicates that the quality classification of upper sandstone for zone II precedes zone I.

Distribution of weak interlayer

A number of thin-layered rock strata are distributed within the thick layer of sandstone in the upper part, which are subjected to weathering leading to the considerable formation of weak interlayered layers paralleling to the surface. These discontinuities have a significant impact on the slope stability because of their unfavorable physical/mechanic properties in terms of shear resistance, and the changes of any types of external boundary conditions (such as excavation and rainfall infiltration) are likely to enable kinematic feasibility. Long-term geological evolution has brought about four well-developed weak interlayers, which, respectively, are designated as JC-1, JC-2, JC-3, and JC-4 from the bottom to top. Their distribution and substance composition are introduced in detail below and summarized in Table 1.

As described in Table 1, the weak interlayers are well developed with a wide range of depths from 2.0 to near 30.0 m and the mechanical properties of each weak layer can be largely altered by water infiltration, triggering motion of potential mass along the weak interlayer surface. It also can be noted that among these four layers, the JC-1 is the most developed in terms of both the thickness and range.

Hydrogeological conditions

The groundwater of the Mayanpo slope is seasonally influenced by rainfall. The overlying Quaternary deposits and weathered sandstone stratum is relatively permeable and can supply the water flow channels. The underlying argillaceous stratum can be considered as an impermeable layer due to its integrity. Therefore, groundwater table can present in the Quaternary deposits and weathered sandstone stratum perching on the relative impermeable argillaceous bedding surface, and the water can accumulate within the vertical tension cracks during wet seasons.

The area is situated in a subtropical zone and has a continental climate influenced by monsoons. Rainfall is mainly concentrated from May to October. Figure 4 shows the distribution of daily rainfall in 2006 recorded at the Yibin meteorological station, which is the nearest one to the Mayanpo slope. From Fig. 4, it can be seen that the accumulated rainfall from May to November accounted for more than 80% of the total rainfall. The intensive rainfalls concentrately occurred in August–September, during which increase of groundwater level is likely to happen.

Deformation characteristics

In the early stage of construction on the Mayanpo slope in June 2006, the excavation has destroyed the equilibrium condition at several sections of the slope, which leads to local collapses and some cracks on the surface according to the descriptions of eye witnesses. Some temporary treatment measures (such as slope cutting and support) were implemented to suppress further expansions of kinematic release. However, with the continued construction, some evidence of unstable state appeared again, especially after a period of concentrated rainfall, for example, (i) the significant amount of deformation, (ii) the propagation of existing cracks, and (iii) the generation of new cracks. Simultaneously, a time-dependent effect that obviously presented progressive propagation of shear surface exists, which can be observed by the creep deformation (surface deformation and deep deformation) and the evolution of surface cracks. In the following section, through the use of a field investigation and recorded inclinometer and surface monitoring data (the layout of monitoring points are shown in Fig. 2(a)), the deformation evolution process and potential failure modes will be studied in depth.

Deformation characteristics based on monitoring history

The monitoring of deformation at the surface of the ground and at depth underground has been carried out since October 2006 (it is worth noting that construction interferences have led to the fluctuation of the measured deformation both on the ground surface and underground). Figure 5 records the surface deformation history of P03, P10, P18, and P15 from October to November 2006. The magnitude of creep deformation keeps increasing continuously with a relatively stable rate. The deformation occurred generally towards to the Mayan gully (X-direction and more than 30 mm for some points). It can be easily seen that the magnitudes of creep deformation in zone I (Fig. 5(c, d)) are much higher than those observed in zone II (Fig. 5(a, b)).

As described in Fig. 6(a, b), the evolutionary process of the monitoring inclinometer data for I02 (zone II) and I08 (zone I) exhibits a similar trend, which can be divided into three segments over depth. First, from the depth of the inclinometer orifice to a depth of approximately 19.5 m, the deformation is relatively uniform over depth at each time, which reflects the deformation integrally. Based on these regularities, this segment constitutes

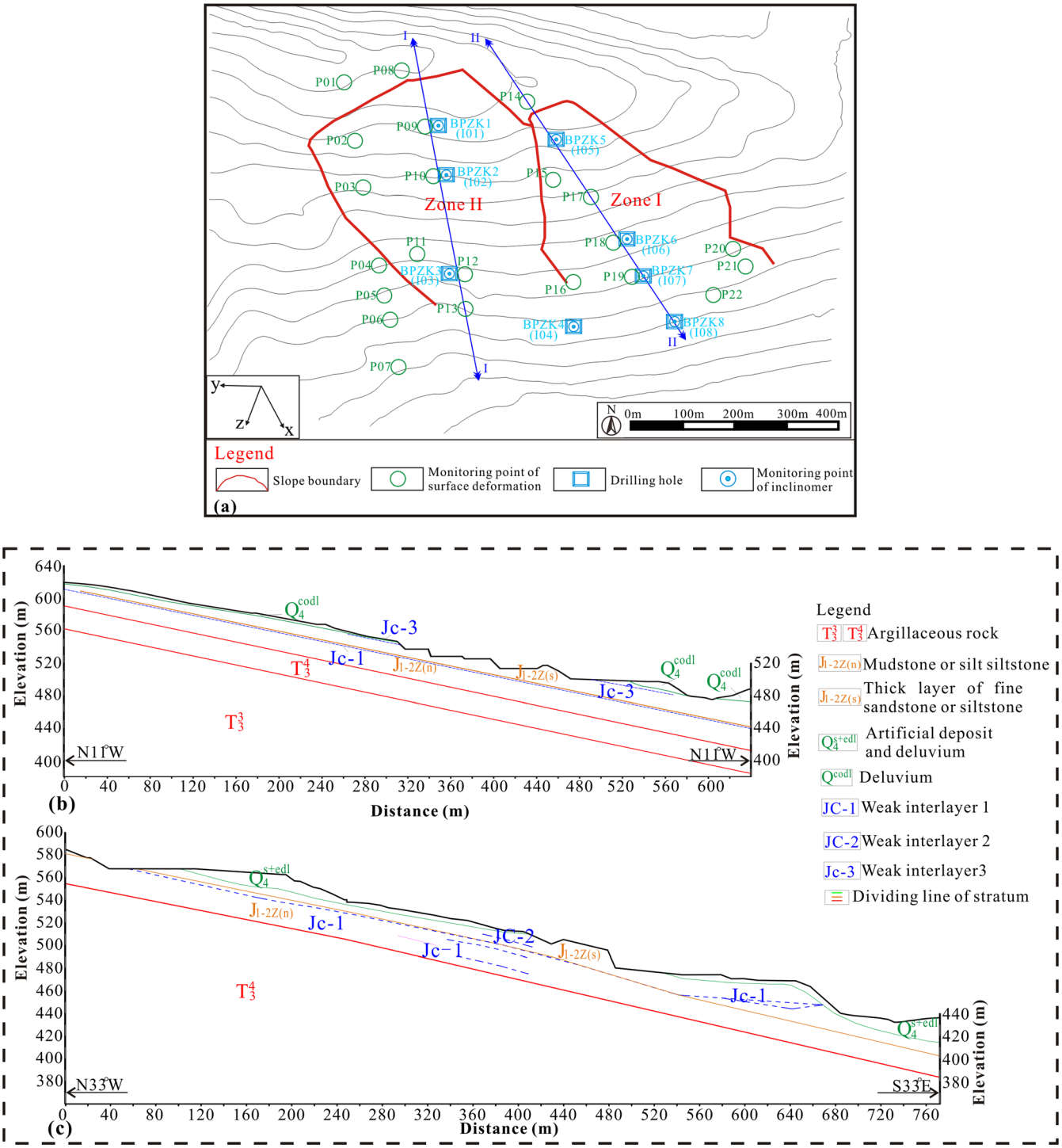

Fig. 2 Geological conditions of the Mayanpo slope: (a) geological ichnography of the Mayanpo slope, also including the monitoring point and drilling position, (b) cross section I and (c) cross section II

mainly the creep-sliding mass. The second segment is located from the depth of 19.5 to 23.5 m, which is the creep-sliding zone due to its characteristics that are common to those in the study of Yin et al. (2016a). The cumulative displacements at each time decrease dramatically from the depth of 19.5 to 21 m and continue to decrease with a slower rate down to the depth of 23.5 m, where the displacements are null; the thickness of this zone keeps constant over time; the increase rate of deformation exhibits a trend of decrease from top to bottom, which indicates the sliding zone suffered progressive degradation in the direction of depth; furthermore, according to the depth of the sliding zone and the buried depth of the weak interlayered layers, it can deem that both the

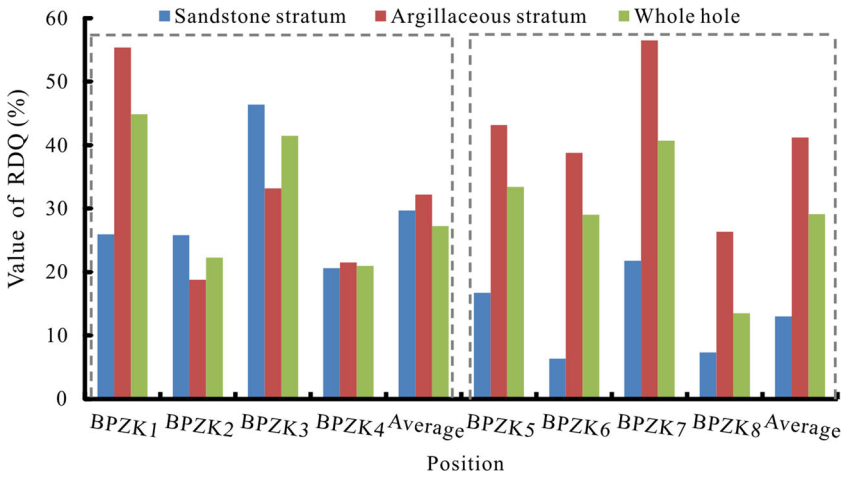

Fig. 3 Distribution of the RQD values for zones I and II

sliding zone of zone I and zone II are controlled by JC-1. The last segment at the depth greater than 23.5 m exhibits almost no cumulative displacement, and remains stable during the monitoring period.

Distribution of crack zones

During the process of slope surface geological investigation, more than 200 cracks were explored that can be classified into 12 fracture zones. Their location and characteristics are marked in Fig. 7. As seen from Fig. 7, the long-term observation of the discovered 12 crack zones indicates that the evolutionary process of the crack zones differs in space and is affected by external disturbances. In zone II and the mountaintop, the crack propagation velocity was 0.5–1.0 mm/day without rainfall, while when raining, the velocity increased to 1.0–2.0 mm/day; a high velocity of 2.3 mm/day was observed at several monitoring positions during downpours. It is also observed that tension crack in zone I became increasing than that in zone II. The average velocity of crack propagation in October was 1.6–2.0 mm/day, whereas the velocity switched between 2.0 and 3.0 mm/day during raining season and 1.0–2.0 mm/day during dry season. Moreover, there exists a zone where tensile fractures distributed intensively which is on the trailing edge of zone II and the dividing line between the two regions (including the south side of the pool and the top of the slope, side slope, and

Table 1 Distribution of the weak interlayers in the Mayanpo slope

Weak interlayer	Thickness (m)	Property	Location of distribution
JC-4	0.25	Gray and brown yellow mudstone and its weathered argillite with characteristics of presenting flow plastic and plastic state meeting water	Back side slope at EL. 554 m
JC-3	0.1–2.0	Gray and brown yellow mudstone and its weathered argillite with characteristics of presenting flow plastic and plastic state meeting water	Back side slope at EL. 575 m; BPZK2 (7.0–7.1 m); BPZK4 (4.6–4.8 m); Back side slope at EL. 500 m and EL. 520 m platform
JC-2	0.05–0.5	Gray white and brown mudstone fragments and its weather argillite that can be pinched into mud powder and has strong viscosity meeting water	BPZK1 (5.4–6.5 m); BPZK2 (12.8–13.1 m); BPZK3 (5.1–5.5 m); Slope of semi-finished material yard
JC-1	0.2–6.4	Gray silty mudstone and fragments of argillaceous siltstone mixed with light gray mud, which is formed by weathering of Argillaceous rocks, presents a loose structure, can be pinched into mud powder, and has strong viscosity meeting water	Excavation slope of substation; pool slope at EL. 500 m; SW slide of the excavation slope at EL. 456 m; BPZK1 (14.4–16.2 m); BPZK2 (19.2–21.9 m); BPZK3 (15.6–18.1 m); BPZK5 (23.0–29.4 m); BPZK6 (10.8–15.9 m); BPZK7 (19.1–21.4 m); BPZK4 (23.6–23.8 m); BPZK8 (27.2–29.6 m)

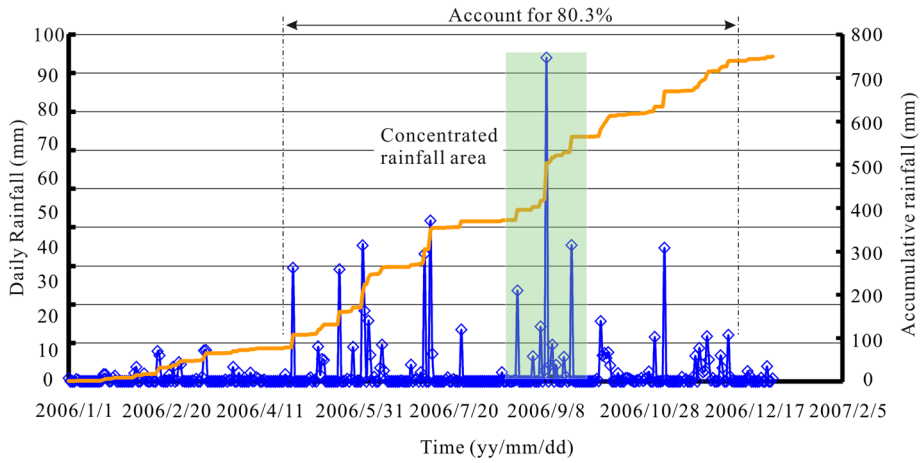

Fig. 4 Distribution of daily rainfall and cumulative rainfall from August to October in 2006 at the Yibin meteorological station

inside of the switch station), and the maximum crack tension width and depth on the south side of the pool reached 80 cm and 10 m, respectively.

In addition to the differences in the evolutionary characteristics of the cracks, the distribution of cracks between zone I and zone II also differed. As shown in Fig. 7, the distribution of the crack zone in zone I was relatively dispersed, most of which are concentrated only in the lower part of the slope and presented a cascade distribution. However, in zone II, those crack zones were only located on the boundary of zone II and exhibited a zonal distribution, which cut zone II as a whole.

Geomechanics model of slope deformation and failure

During different stages including the evolution of deformation, initiation of sliding, and ultimate failure of slope, external disturbances play different roles in the redistribution of stress regime that is closely related to the gradual development of sliding zone in a progressive manner, leading to its coalescence and eventual failure (Eberhardt et al. 2004; Xu et al. 2015). However, even the triggering factors are more or less the same, diversities of macroscopic response process (i.e., deformation) can still occur due to different geological settings, which determines the final failure. The different creep deformation characteristics observed between zone I and zone II are indeed closely associated with the different quality of upper rock stratum, which not only depressed the formation and propagation of cracks but also blocked rainfall infiltration channel, implying that geomechanical modes of potential failure for two zones will be occurring in different manners.

Firstly, we present a geomechanical deformation-failure model for slope in zone I (Fig. 8(a)). The free face formed by undercutting without reinforcement had an adverse impact in driving the slope towards a disequilibrium/unstable state, which induced possibility of kinematic release. In addition, owning to broken weathering sandstone stratum, it is hard for sliding mass to maintain integrity during creep because of the maximum tensile stress on the surface is high enough to crack the rock and induce new ruptures. Meanwhile, cracks not only create new free space for the posterior sliding mass leading to the formation of multi-stage sliding masses, but also serve as channels for infiltration of rainwater. The infiltration of water has resulted in the progressive degradation of material of the sliding mass and sliding zone, which, in turn, accelerated the rate of crack expansion and shearing. This can be confirmed by the appearance of a sub-slip surface. Overall, with continuous propagation and coalescence of the main-slip and sub-slip surfaces, zone I presents multistage creep-fracturing progressive deformation-failure mode.

Pulled by zone I and also disturbed by excavation and rainfall, the initial equilibrium condition is broken to enable kinematic feasibility. As shown in Fig. 8(b), unlike zone I, more integrated sandstone stratum for zone II has a significant effect to suppress the formation of extrusive crack on the sliding mass without occurrence of sub-slip surface in zone II. There are only several cracks that are mainly concentrated in trailing edge of the slope. The sliding mass was observed to be creeping along the main-slip surface (i.e., JC-1), and rainfall infiltration also plays a role in accelerating the rate of creep and interlaminar shear, resulting in predominant development of main-slip surface for gradual failure. Overall, zone II presents integral creep-fracturing progressive deformation-failure mode.

Mechanism analysis

Well understanding for the mechanisms of deformation process in response to the internal and external triggering factors is of importance for hazard prevention and mitigation. In general, unloading-induced rebound and creep are main types of slope deformation. The deformation and displacement accumulate preceding an eventual failure which requires the formation of sliding surface, and external disturbance can result in the expansion of interlaminar shear to promote this cumulative process. Clearly, the creep deformation in this study is considered to be the endogenic and exogenic integration, and we ensure that the engineering excavation and rainfall infiltration are triggering factors when coupling unfavorable geological conditions. In this section, some further points will be introduced, especially regarding to the evolutional process of predominant discontinuity and the responding mechanism of excavation/rainfall-induced planar sliding.

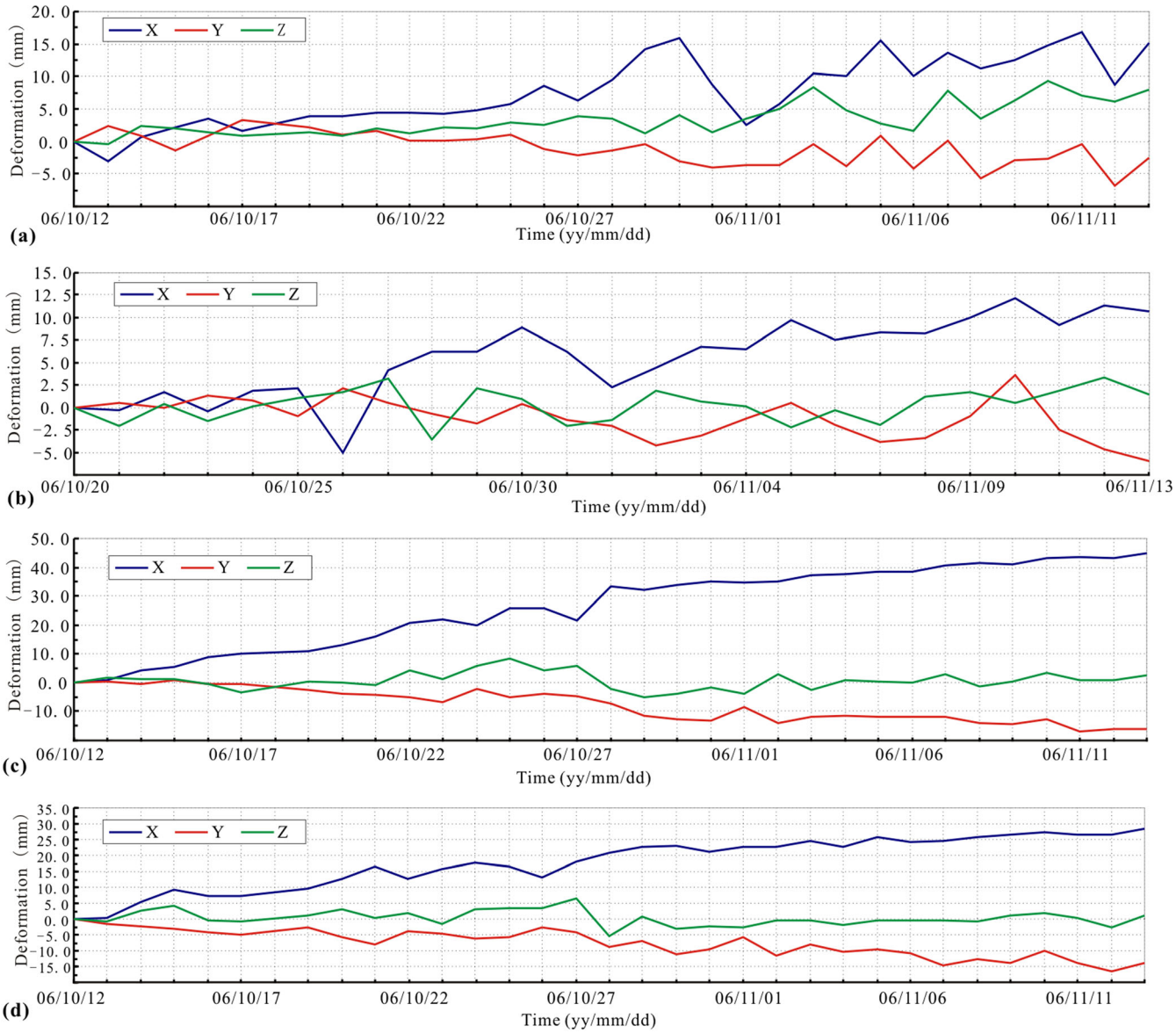

Note: The positive direction of X, Y and Z are corresponding to Fig. 2a.

Fig. 5 Surface deformation histories from October to November: (a) P03; (b) P10; (c) P18 and (d) P15

Progressive formation of predominant discontinuity

From the engineering practice, it is known that the sedimentary stratum behaves anisotropically that is influenced by bedding planes which act as weak surface. A predominant plane emerges and occurs as the slip surface (Stead and Wolter 2015), which is a long-term process, and unusually accompanied by the progressive degradation of mechanical properties of the predominant discontinuity. This process includes several stages from the primary soft rock stratum to an entire sliding zone (Hatzor and Levin 1997; Shuzui 2001; Wen and Aydin 2005; Li et al. 2007; Xu et al. 2010, 2014).

Original sub-horizontal beds were uplifted, titled, and folded under the action of tectonic movement. This has resulted in bedding planes dipping out of the slope and the formation of interbedded argillaceous stratum and sandstone stratum where thick-layered sandstone stratum is mixed with thin-layered sandstone. This early topography presented a relatively stable state (Fig. 9(a)). However, the thin-layered stratum exhibited a low resistance to weathering which is considerably soft in comparison with the surrounding thick lithology. Under long-term weathering, rock stratum will be subjected to progressive degradation in strength and other mechanical properties, due to the gradual alterations in molecular structure, mineral composition, and microscopic contact mode (i.e., more and more loose, porous, and more content of clay mineral) (Zhang et al. 2016). The degree of strength degradation differs depending on the rock types, which would be apparently more significant in the soft thin-layered stratum (Hatzor and Levin 1997; Eberhardt et al. 2004; Li et al. 2007; Xu et al. 2016). Meanwhile, the gravitational

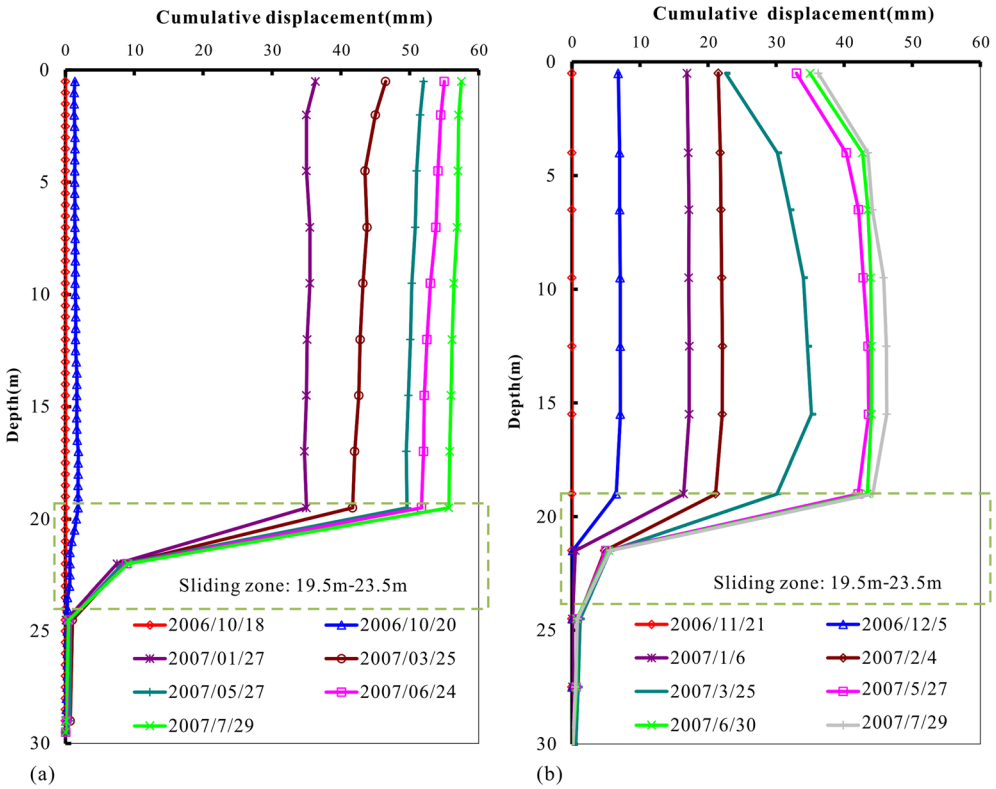

Fig. 6 Historical displacement monitoring data from different inclinometers in the Mayanpo slope: (a) I02 and (b) I08

force drives the slope towards an unstable state, exhibiting a downward sliding trend along the predominant degraded primary soft rock. This external force, combined with internal degradation, has resulted in shearing deformation and interlaminar shearing. Besides, the groundwater fluctuation had a further adverse effect and accelerated the process of interlaminar shear, as shown in Fig. 9(b). Generally, induced by interlaminar shear, other alteration occurs in the primary

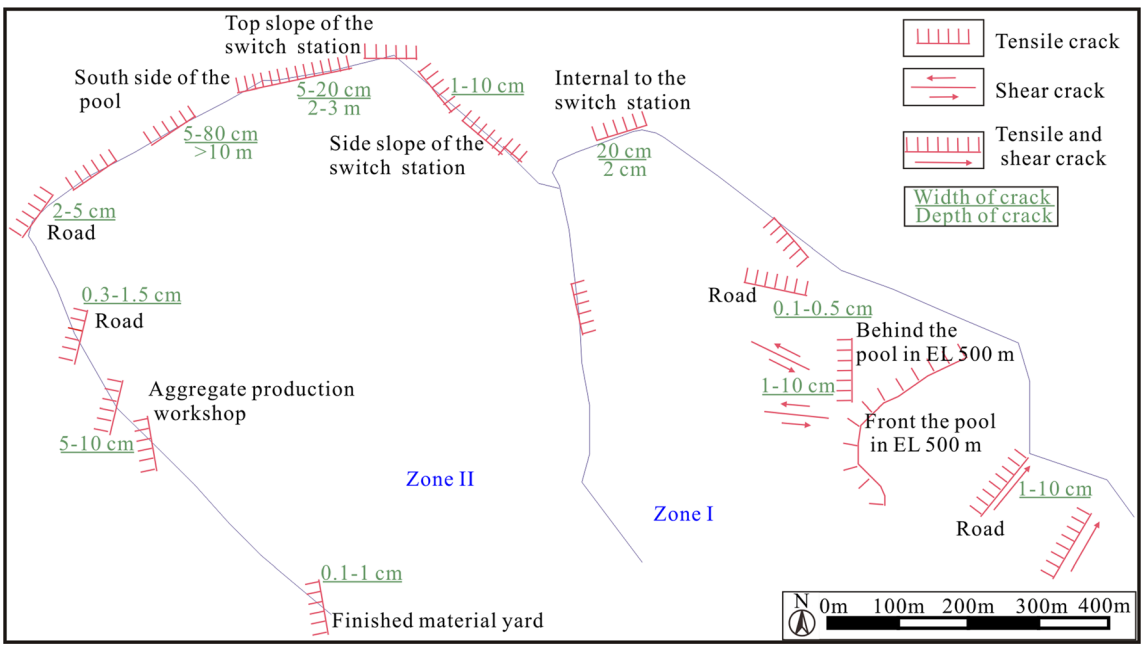

Fig. 7 Distribution characteristics of crack zones in the Mayanpo slope

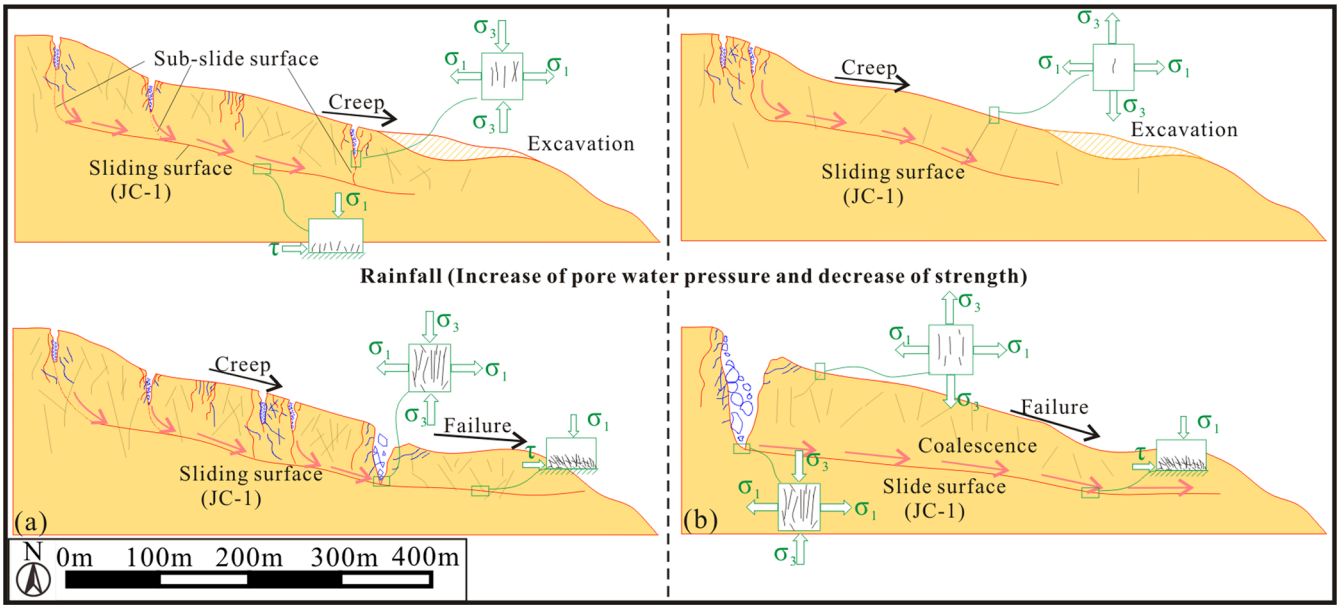

Fig. 8 Deformation-failure modes for zones I and II, respectively: (a) zone I; (b) zone II

soft rock, such as argillization, which gradually evolves into an interlayer shear zone serving as a weaker interlayer or predominant discontinuity (Li et al. 2007); as indicated by geological survey, there are four weak interlayers developed in the Mayanpo slope. Although some local failures (such as small collapse) may occur because of just kinematic release of some points, the slope is still in an equilibrium condition, as show in Fig. 9(c). Without disturbance, this slope will not undergo rapid sliding due to full persistence of discontinuities, but both excavation without support and rainfall infiltration have led to various changes, including the flow and stress regime in the slope, as well as the material properties.

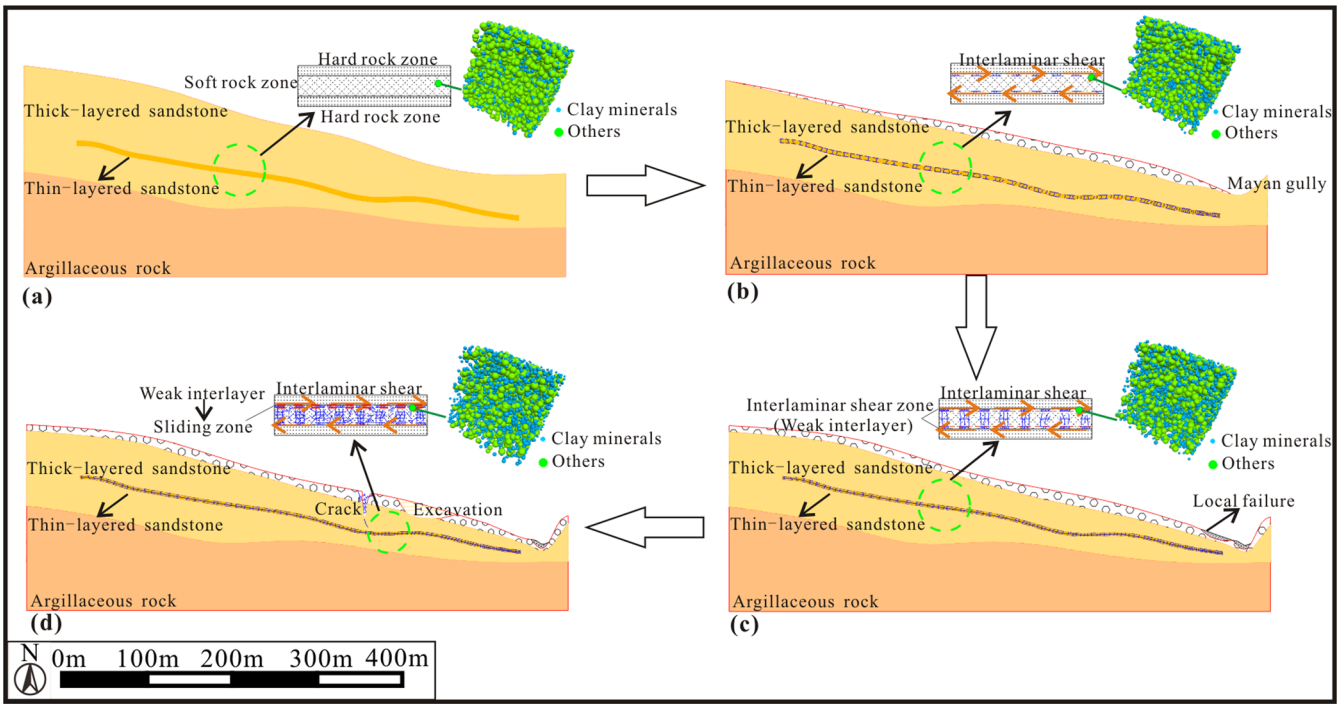

Fig. 9 Evolutionary process of the dominant interlayer: (a) initial soft rock distribution; (b) formation of interlaminar shear; (c) evolution of the dominant interlayer; (d) gradual evolutionary process of the sliding zone after excavation and rainfall

As shown in Fig. 9(d), the resulted interlaminar shearing plays a vital role in promoting the propagation of predominant discontinuity and leads to obvious creep deformation.

Response characteristics under excavation-rainfall condition

As proposed by Zhou et al. (2016), the deformation and failure of slope mostly experience long-term evolution and short-term effects. As observed in the Mayanpo slope, long-term interlaminar shearing associated with tectonism contributed significantly to the progressive formation of four weak interlayers, while disturbance by excavation without support and rainfall in short term enabled kinematic feasibility of potential failure mass. The respond characteristics subjected to short-term disturbance can be investigated by various numerical simulations, as indicated in the review made by Stead et al. (2006). In this study, a numerical investigation based on hydromechanical FEM is implemented to investigate the mechanism of the Mayanpo under the excavation-rainfall condition.

Numerical model

Section II (indicated in Fig. 2(a)) is chosen as the typical profile for calculation; the FDM model is mapped as shown in Fig. 10(a) (the accumulation layer on the surface has been simplified into the sandstone stratum because of thinner thickness). This section was subjected to two large-scale excavation disturbances, respectively, induced by finished material yard and semi-manufactured material yard. After the completion of first excavation, the effect of rainfall infiltration is considered by the increase of pore water pressure and the decrease of strength. The groundwater level was proposed to rise by about 5 m by Hydro-China Zhongnan Engineering Corporation (HCZEC 2007), as described by Fig. 10(a). Furthermore, a series of experimental tests and inversion analysis on the shear strength parameters have been conducted by the designer (HCZEC 2007). These required parameters are summarized in Table 2. In addition, the material in sliding zone also exhibits the characteristics if strain softening (Ghazvinian et al. 2010; Hu et al. 2017), which is considered by using an extended Mohr-Coulomb model in this study. As shown in Fig. 10(b), before reaching the peak state, the stress-strain relation is described by the conventional Mohr-Coulomb constitutive model. However, in the post-peak state, the model assumes that both shear strength parameters (i.e., the cohesion, c, and the friction angle, ϕ) reduce from the peak to residual values in a linear manner with the accumulation of plastic shear strain (Zhang et al. 2013; Qi and Vanapalli 2016). Some parameters (including c_r, ϕ_r, ε_p, and ε_r) cannot be determined by the designer (HCZEC 2007), and we just reference similar project summarized in the doctoral thesis of Zheng (2008), where the strain softening features of different types of weak interlayer have been explored. Additional element (including J and T in Fig. 10(a)) is described by the classic Mohr-Coulomb constitutive model.

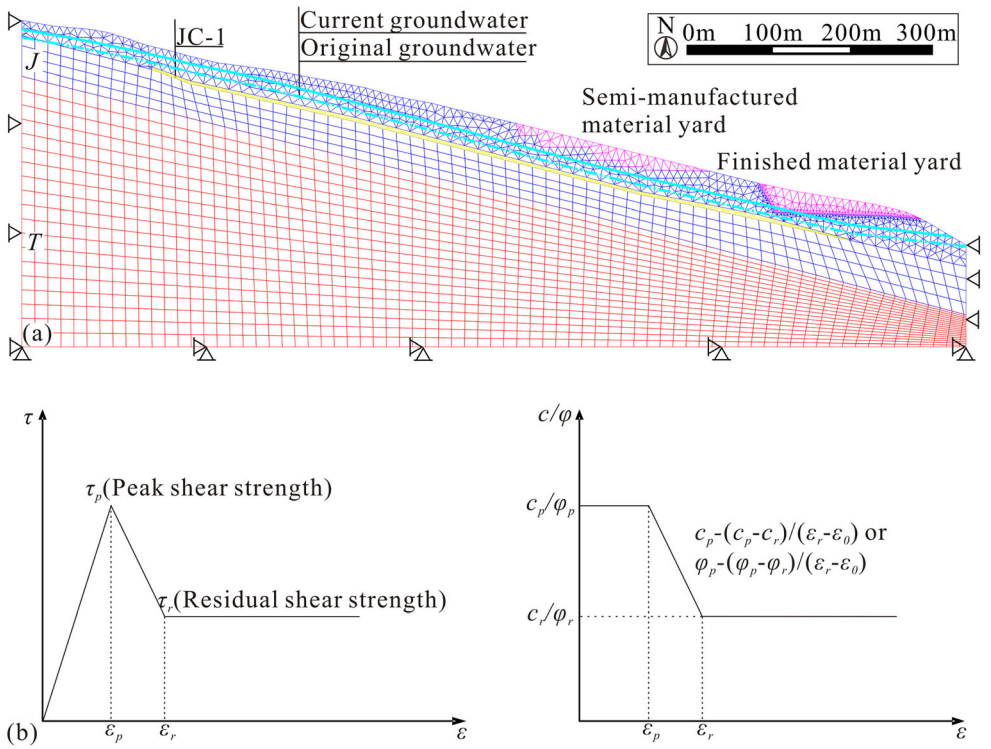

Fig. 10 Numerical simulation model of the Mayanpo slope: (a) two-dimensional hydromechanical FDM information; (b) extended Mohr-Coulomb constitutive model via a consideration of the post-peak stress-strain relation

Table 2 Mechanical parameters of different strata in the Mayanpo slope

Stratum	Density (kg/m^3)	Tensile strength (MPa)	Elastic modulus (GPa)	Poisson's ratio	c_p (MPa)	ϕ_p (°)	c_r (MPa)	0
J	2500 (2600)	0.12 (0.11)	10	0.24	0.3 (0.288)	30 (29)	ϕ_r (°)	8
JC	1700 (1900)	0.004	0.1	0.31	0.01 (0.007)	15 (12)	ε_p	0
T	2552 (2552)	0.156 (0.156)	16	0.23	0.39 (0.39)	41.3 (41.3)	ε_r	0.3

The parameters inside and outside the parentheses represent the calculation conditions after rainfall and before rainfall, respectively. Some of the parameters involved in strain softening are only applied to JC

Numerical results

Figure 11(a–c) presents the calculation results after the first excavation. As shown in Fig. 11(a), the value of maximum horizontal displacement reaches to about 1 cm near the trailing edge of the slope, which is primarily induced by excavation that provides kinematic feasibility and sliding mass moves along JC-1. Further, creep deformation promotes the effect of interlaminar shear, which leads to (i) large shear strain increment along JC-1 (Fig. 11(c)), (ii) formation of a significant tensile strain concentration zone in the trailing edge without coalescence as gradient strain increment (Fig. 11(b)), and (iii) very small shear strain in the trailing edge (Fig. 11(c)). After rainfall, decreasing strength and increasing pore water pressure result in substantial horizontal displacement (Fig. 11(d)), which is larger than 2 cm and in a good agreement with the measurement. This creep process results in increases of both maximum principle strain increment and maximum shear strain increment (as shown in Fig. 11(e, f)). By comparing before and after rainfall, the sliding zone along JC-1 and tensile strain concentration zone in the trailing edge are ceaselessly propagating under tension-shear destruction.

Discussions

Considering the seriousness of creep deformation for the Mayanpo slope, engineering prevention and control were suggested to be divided into two phases. The objective of the first phase was to immediately suppress the continuous deformation. The specific measures, aimed at location of the serious deformation, included the use of (i) prestressed anchor cables (PAC), (ii) anti-slide piles (AP), and (iii) drainages and backfills in all cracks. The second phase measures were employed after the completion of the first phase, which were aimed to

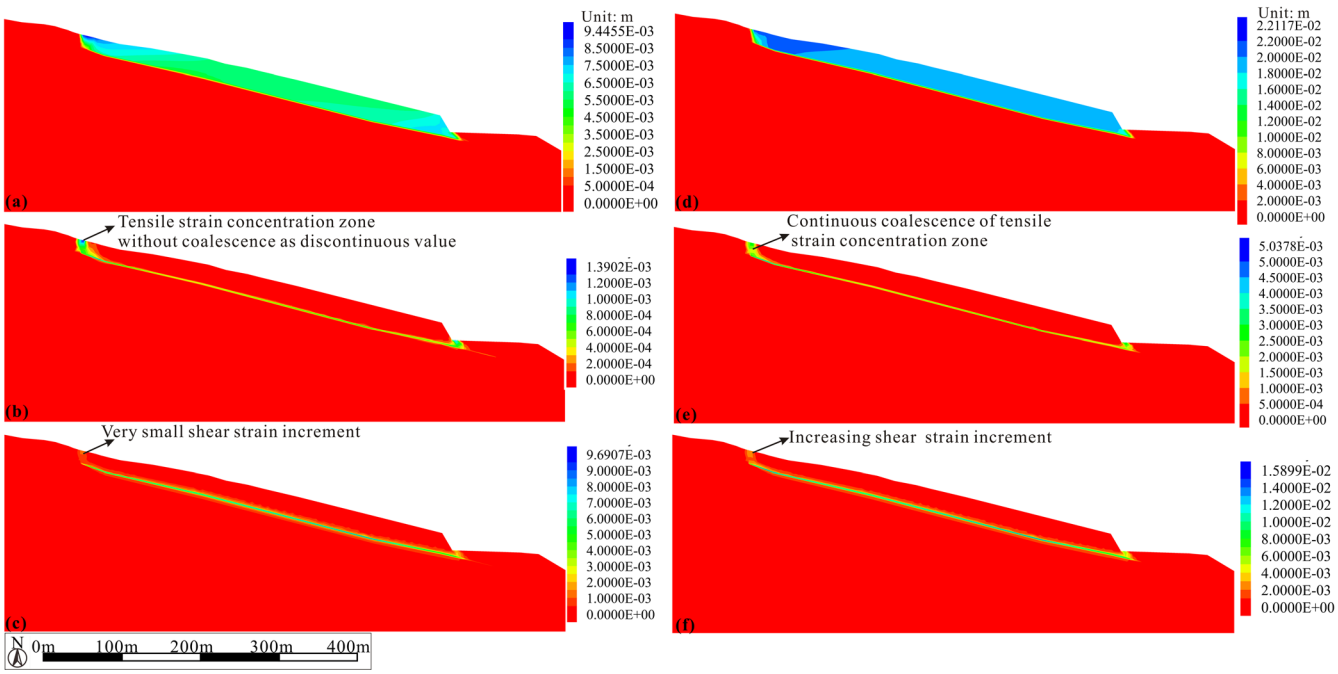

Fig. 11 Numerical simulation results: (a) horizontal deformation after first excavation; (b) maximum principal strain increment after first excavation; (c) maximum shear strain increment after first excavation; (d) horizontal deformation after rainfall; (e) maximum principal strain increment after rainfall; (f) maximum shear strain increment after rainfall

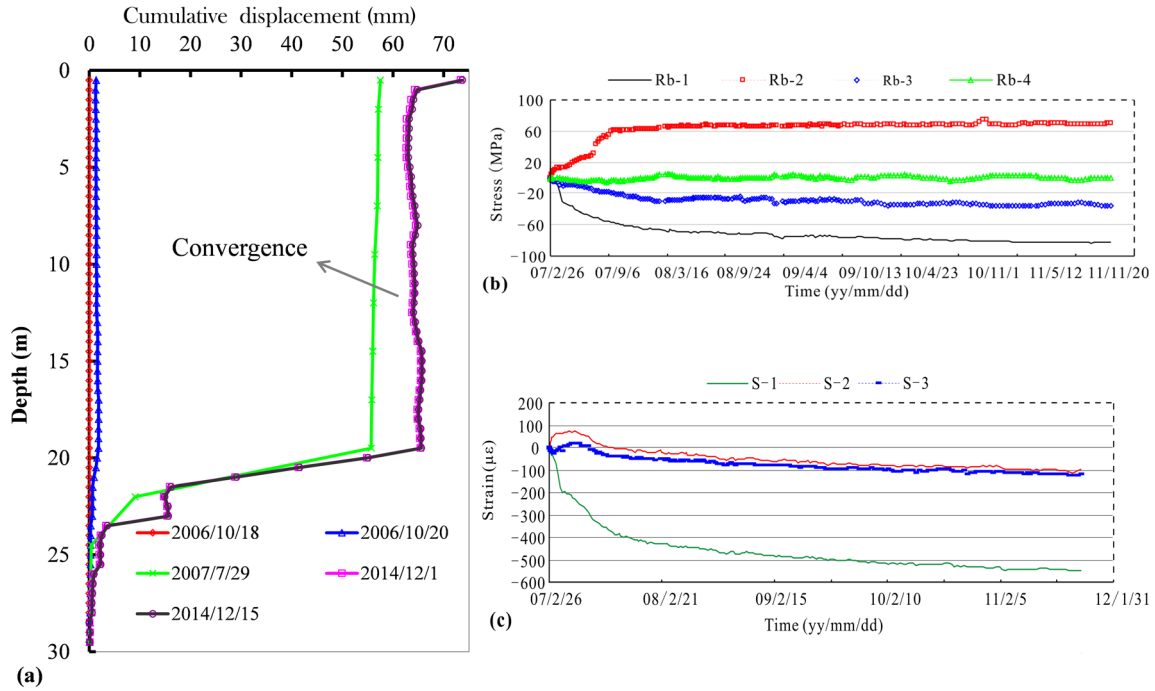

Fig. 12 Typical monitoring results of displacement, stress, and strain after prevention and control: (a) Monitoring inclinometer data for I02; (b) stress change for a steel bar in the anti-slide pile around the switch station (3 measurement points); (c) strain change in anti-slide pile concrete around the switch station (3 measurement points)

improve the stability and to ensure long-term safety. The specific measures mainly included slag, AP, and the improvement of drainage system. After the completion of these two phases of engineering prevention and control, the deformation tendency, stress, and strain presented converging trends, as shown in Fig. 12.

As can be seen from this massive bedding rockslide, the evolutionary process of the predominant discontinuities determines the development of the slope stability. All of the exogenic influences will have an impact on the interlaminar shear (acceleration or deceleration), as indicated by the Mayanpo slope based on the numerical investigation and other similar projects (Haruo 2001; Wen and Aydin 2005; Tang et al. 2015), which directly and indirectly contributes propagation of predominant discontinuities. Thus, the main goal of prevention and control should be concentrated on suppressing interlaminar shear through drainage (Yin et al. 2016b), deep supports (Hu et al. 2017), cutting slopes, and backfills (Jiang et al. 2016).

Conclusions

In this study, a project at the Xiangjiaba Hydropower Station, named as the Mayanpo massive bedding rock slope, is used as an example to systematically investigate the geological settings, deformation characteristics, potential failure modes, triggering mechanism, and prevention of massive bedding rockslides, typical type of planar sliding. Some conclusions can be drawn:

The Mayanpo slope, which can be divided into two zones, i.e., east zone (labeled as zone I) and west zone (labeled as zone II), is a typical monoclinic stratum and exploits a formation of interbedded mudstone and sandstone mixed with four weak interlayers, and these bedding planes are approximately parallel to the surface. According to the recorded inclinometer monitoring data, JC-1 is deemed to be the predominant discontinuity. Both the surface deformation and the distribution of crack zones indicate the diversity between zones I and II, reflected in the deformation magnitude and deformation-failure mode, which are closely sensitive to the quality of upper rock stratum. The deformation in zone I is obviously larger in magnitude than zone II. The geomechanic models of deformation and failure in zone I and II, respectively, present multistage and integral creep-fracturing progressive deformation-failure mode.

The mechanism of deformation can be considered to be a consequence of the endogenic and exogenic integration. The progressive evolution of predominant discontinuity from primary soft rock stratum (thin-layered sandstone stratum) to weak interlayer is the fundamental, which provides the possibility of kinematic release. As indicated by hydromechanical FDM analysis considering the stress-strain relation in post-peak stage, excavation without reinforcement enables kinematic feasibility, leading to creep and shear along JC-1 and formation of a tensile strain concentration zone in the trailing edge. During rainfall, decreasing strength and increasing pore water pressure have accelerated the horizontal displacement, resulting in the increase of maximum principle strain increment and maximum shear strain increment. A tensile strain concentration zone in the trailing is formed and ceaselessly propagating under tension-shear effect. The prevention and control measures are implemented, including prestressed anchor cables, anti-slide piles, drainages, and backfills in all cracks, and the core of these measures is concentrated on the suppression of interlaminar shear.

Acknowledgements

Critical comments by the two anonymous reviewers greatly improved the initial manuscript.

Funding information

This study received funding from the National Key R&D Program of China (2017YFC1501102), National Natural Science Foundation of China (41472272), and the Youth Science and Technology Fund of Sichuan Province (2016JQ0011).

References

Cruden DM, Antoine P (1984) The slide from Mt. Granier, Isére and Savoie, France on Nov. 24, 1248. In: Proceeding of the 4th international symposium on landslides, Toronto, Vol 1, pp 475–481

Eberhardt E, Stead D, Coggan JS (2004) Numerical analysis of initiation and progressive failure in natural rock slopes—the 1991 Randa rockslide. Int J Rock Mech Min Sci 41:69–87

Eberhardt E, Thuro K, Luginbuehl M (2005) Slope instability mechanisms in dipping interbedded conglomerates and weathered marls—the 1999 Rufi landslide, Switzerland. Eng Geol 77:35–56

Ghazvinian AH, Taghichian A, Hashemi M, Mar'ashi SA (2010) The Shear Behavior of Bedding Planes of Weakness Between Two Different Rock Types with High Strength Difference. Rock Mech Rock Eng 43(1):69–87

Hart MW (2000) Bedding-parallel shear zones as landslide mechanisms in horizontal sedimentary rock. Environ Eng Geosci 6:95–113

Haruo SZ (2001) Process of slip-surface development and formation of slip-surface clay in landslides in tertiary volcanic rocks, Japan. Eng Geol 61:199–220

Hatzor YH, Levin M (1997) The shear strength of clay-filled bedding planes in limestones-back-analysis of a slope failure in a phosphate mine, Israel. Geotech Geol Eng 15:263–282

Havaej M, Stead D (2016) Investigating the role of kinematics and damage in the failure of rock slopes. Comput Geotech 78:181–193

Hu QJ, Shi RD, Zheng LN, Du LQ, He LP (2017) Progressive failure mechanism of a large bedding slope with a strain-softening interface. Bull Eng Geol Environ 77:69–85. https://doi.org/10.1007/s10064-016-0996-x

Huang RQ (2007) Large-scale landslides and their sliding mechanisms in China since the 20th century. Chin J Rock Mech Eng 26:433–454 **(in Chinese)**

Hungr O, Leroueil S, Picarelli L (2014) The Varnes classification of landslide types, an update. Landslides 11:167–194

Hydro-China Zhongnan Engineering Corporation (HCZEC) (2007) Research on the stability and reinforcement for the Mayanpo landslide at the Xiangjiaba Hydropower Station. Technical report, pp. 1-165, Changsha. (in Chinese)

Jiang QH, Wei W, Xie N, Zhou CB (2016) Stability analysis and treatment of a reservoir landslide under impounding conditions: a case study. Environ Earth Sci 75:2

Leshchinsky B, Vahedifard F, Koo HB, Kim SH (2015) Yumokjeong landslide: an investigation of progressive failure of a hillslope using the finite element method. Landslides 12:997–1005

Li SD, Li X, Wu J, Liu YH (2007) Evolution process and pattern of sliding zone in large consequent bedding rock landslide. Chin J Rock Mech Eng 26:2473–2480 **(in Chinese)**

Lynn MH, Peter B (2008) The landslide handbook—a guide to understanding landslides. U.S. Geol Surv Circ 1325, 129p

Qi SC, Vanapalli SK (2016) Influence of swelling behavior on the stability of an infinite unsaturated expansive soil slope. Comput Geotech 76:154–169

Roberts NJ, Evans SG (2013) The gigantic Seymareh (Saidmarreh) rock avalanche, Zagros Fold-Thrust Belt, Iran. J Geol Soc 170:685–700

Shuzui H (2001) Process of slip-surface development and formation of slip-surface clay in landslides in tertiary volcanic rocks, Japan. Eng Geol 61:199–220

Stead D, Wolter A (2015) A critical review of rock slope failure mechanisms: the importance of structural geology. J Struct Geol 74:1–23

Stead D, Eberhardt E, Coggan JS (2006) Developments in the characterization of complex rock slope deformation and failure using numerical modelling techniques. Eng Geol 83:217–235

Tang HM, Zou ZX, Xiong CR, Wu YP, Hu XP, Wang LQ, Lu S, Robert EC, Li CD (2015) An evolution model of large consequent bedding rockslides, with particular reference to the Jiweishan rockslide in Southwest China. Eng Geol 186:17–27

Tannant DD, Giordan D, Morgenroth J (2017) Characterization and analysis of a translational rockslide on a stepped-planar slip surface. Eng Geol 220:144–151

Wen BP, Aydin A (2005) Mechanism of a rainfall-induced slide-debris flow: constraints from microstructure of its slip zone. Eng Geol 78:69–88

Xu Q, Fan XM, Huang RQ, Yin YY, Hou SS, Dong XJ, Tang MG (2010) A catastrophic rockslide-debris flow in Wulong, Chongqing, China in 2009: background, characterization, and causes. Landslides 7:75–87

Xu WJ, Jie YX, Li QB, Wang XB, Yu YZ (2014) Genesis, mechanism, and stability of the Dongmiaojia landslide, yellow river, China. Int J Rock Mech Min Sci 67:57–68

Xu L, Dai FC, Chen J, Lqbal J, Qu YX (2015) Analysis of a progressive slope failure in the Xiangjiaba reservoir area, Southwest China. Landslides 11:55–66

Xu Q, Liu HX, Ran JX, Li WH, Sun X (2016) Field monitoring of groundwater responses to heavy rainfalls and the early warning of the Kualiangzi landslide in Sichuan Basin, southwestern China. Landslides 13:1–16

Yin YP, Sun P, Zhang M, Li B (2011) Mechanism on apparent dip sliding of oblique inclined bedding rockslide at Jiweishan, Chongqing, China. Landslides 8:49–65

Yin YP, Huang BL, Wang WP, Wei YJ, Ma XH, Ma F, Zhao CJ (2016a) Reservoir-induced landslides and risk control in Three Gorges Project on Yangtze River, China. J Rock Mech Geotech Eng 8:577–595

Yin YP, Li B, Wang WP, Zhan LT, Xue Q, Gao Y, Zhang N, Chen HQ, Liu TK, Li AG (2016b) Mechanism of the December 2015 catastrophic landslide at the Shenzhen landfill and controlling geotechnical risks of urbanization. Engineering 2:230–249

Yue ZQ, Lee CF (2002) A plane slide that occurred during construction of a national expressway in Chongqing, SW China. Q J Eng Geol Hydrogeol 35:309–316

Zhang K, Cao P, Bao R (2013) Progressive failure analysis of slope with strain-softening behaviour based on strength reduction method. Journal of Zhejiang University SCIENCE A 14:101–109

Zhang S, Xu Q, Hu ZM (2016) Effects of rainwater softening on red mudstone of deep-seated landslide, Southwest China. Eng Geol 204:1–13

Zheng LN (2008) Research of failure mechanism and the local failure zones for consequent slope based on strain softening theory. Doctoral thesis, pp 12–31, Southwest Jiao Tong University, Chengdu. **(in Chinese)**

Zhou JW, Cui P, Hao MH (2016) Comprehensive analyses of the initiation and entrainment processes of the 2000 Yigong catastrophic landslide in Tibet, China. Landslides 13:39–54

Zhou JW, Jiao MY, Xing HG, Yang XG, Yang YC (2017) A reliability analysis method for rock slope controlled by weak structural surface. Geosci J 21:453–467

S.-l. Zhang · S.-c. Qi · J.-w. Zhou (✉)
State Key Laboratory of Hydraulics and Mountain River Engineering,
Sichuan University,
Chengdu, 610065, People's Republic of China
Email: jwzhou@scu.edu.cn

Z.-h. Zhu
China Institute of Water Resources and Hydropower Research,
Beijing, 100038, People's Republic of China

Y.-x. Hu
College of Water Resource and Hydropower,
Sichuan University,
Chengdu, 610065, People's Republic of China

Q. Du
Three Gorges Tibet Energy Investment Co., Ltd, China Three Gorges Corporation,
Lhasa, 850000, People's Republic of China